

7. Data Analysis and Results

The results on the atmospheric neutrino flavour content in Soudan 2 are presented in this chapter. First, the data is divided into ν_e -like and ν_μ -like events by using the energy dependent Λ_{46} cut, which is described in the previous chapter. A background fit is performed on each flavour separately. The Ratio of Ratios is calculated. The atmospheric neutrino anomaly is then discussed in terms of the flavour and zenith angle estimators. Moving a step further, the data is compared to the Standard Model expectation in terms of a *multi-variable fit*, which allows for the presence of background in **GOLD**. Finally the multi-variable fit is used in testing the $\nu_\mu \leftrightarrow \nu_e$, $\nu_\mu \leftrightarrow \nu_\tau$ and 3-generation maximal mixing [51][52] hypotheses against the data.

7.1 Atmospheric Neutrino Anomaly Revisited

This section deals with the calculation of the Ratio of Ratios (see Table 2.2), a figure much loved in atmospheric neutrino experiments:

$$R = \frac{\left[\nu_\mu \text{-like} / \nu_e \text{-like} \right]_{data}}{\left[\nu_\mu \text{-like} / \nu_e \text{-like} \right]_{MC}} \quad (7.1)$$

It is known that the **GOLD** data sample is contaminated by non-neutrino interactions at the level of 30% (§5.6.3). In the calculation of R the effect of the background must be subtracted from the data. This can be achieved by either of the following methods:

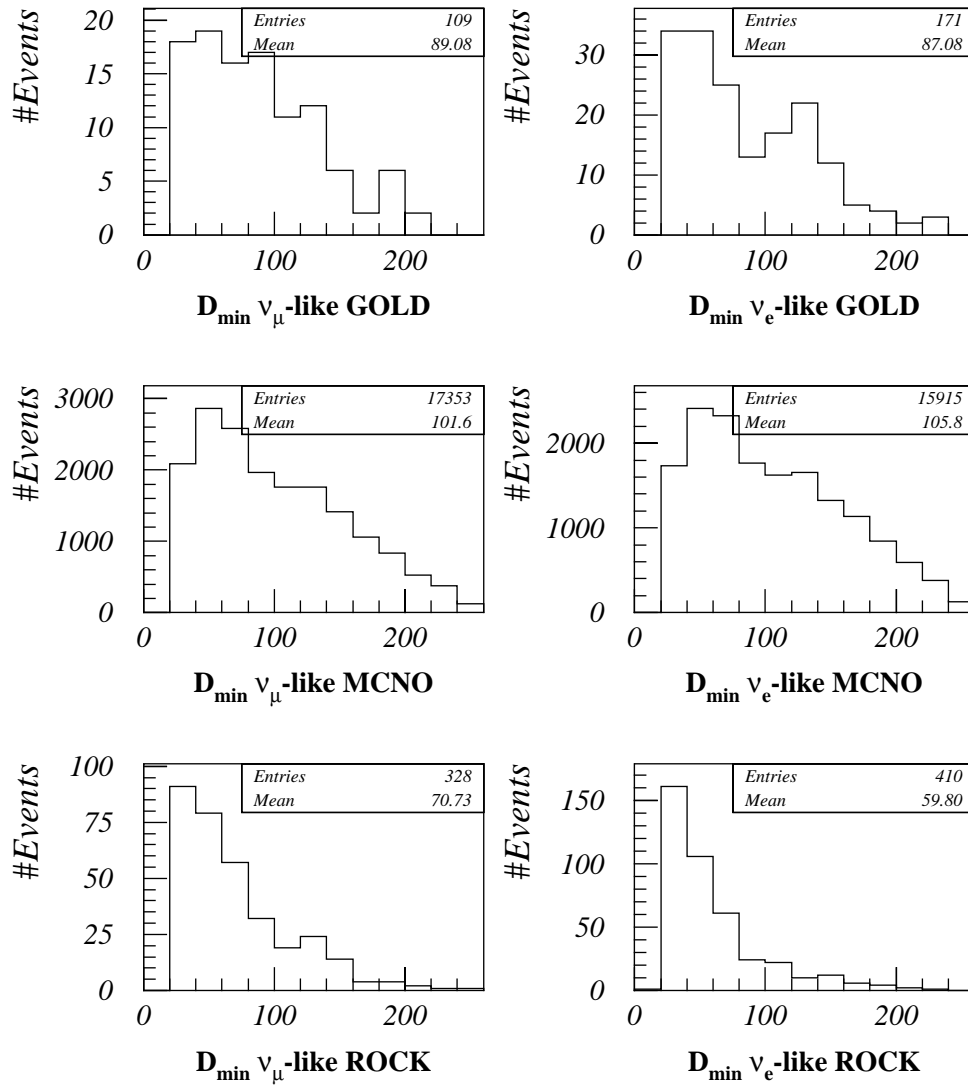
- The neutrino count and background contamination of the complete **GOLD** sample can be calculated, as in §5.6.3. The flavour content of the **GOLD** neutrino and

background samples can then be estimated from the flavour compositions of the **MCNO** and **ROCK** event samples.

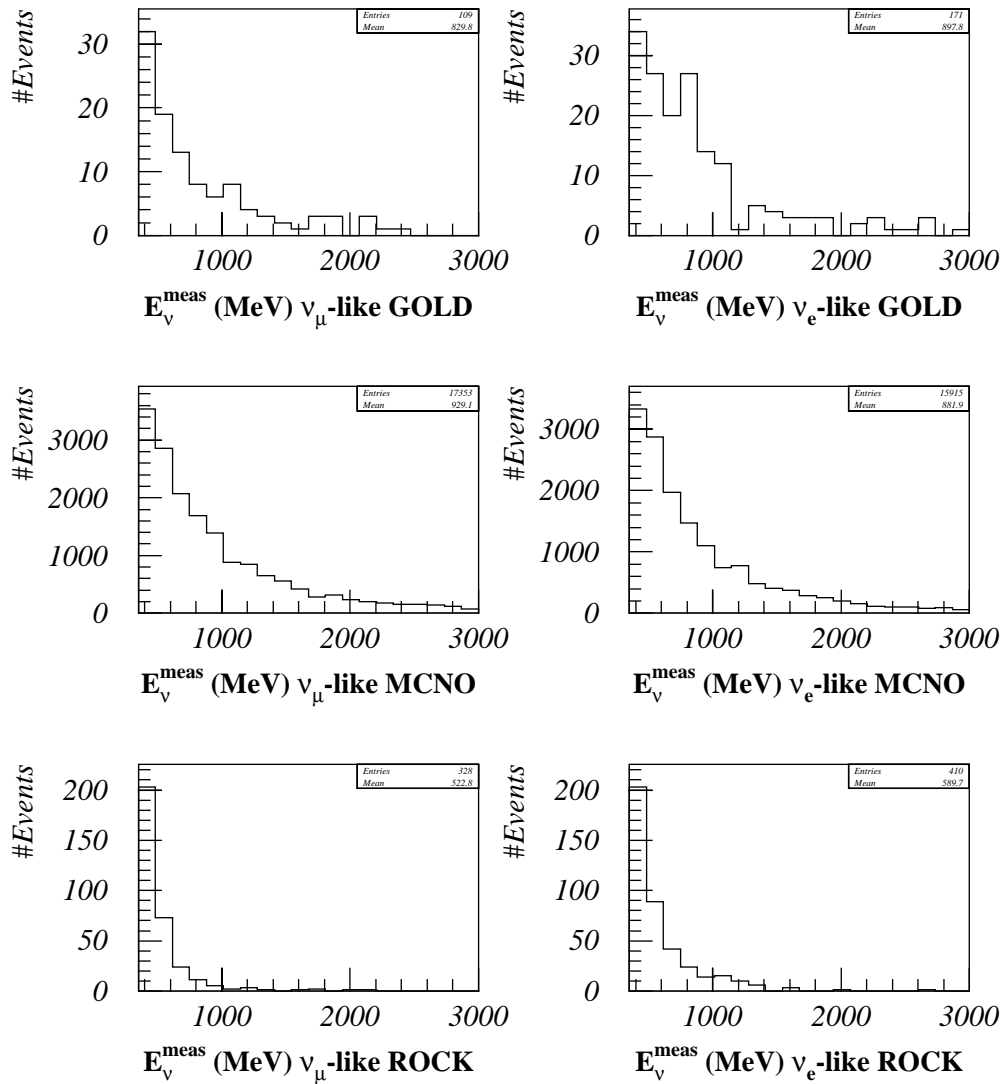
- Alternatively, the **GOLD**, **MCNO** and **ROCK** events samples can be divided into ν_e -like and ν_μ -like samples, using the Λ_{46} - N_{Hits} cut as described in the previous chapter. The background calculation can be performed for each flavour separately. The numbers of ν_e -like and ν_μ -like **GOLD** neutrino events can be fed into the calculation for R . The errors on the numbers of ν_e -like and ν_μ -like **GOLD** neutrino events are uncorrelated and can simply be added in quadrature.

The latter of the two methods will be adopted here. Its main advantage is that it takes into account differences that exist in the distributions of Depth (§5.3.2) and Energy (§6.3) between **ROCK** (background) ν_e -like and ν_μ -like events. In particular, ν_e -like **ROCK** events are mainly due to photons and, because of the ≈ 15 cm radiation length in Soudan 2, materialise near the outside of the detector. On the other hand ν_μ -like **ROCK** events are typically short proton tracks produced by neutrons (and other neutral particles) and often appear deep inside the detector – the hadron interaction length in Soudan 2 is ≈ 80 cm. This is observed in the Depth distributions of ν_e -like and ν_μ -like **ROCK** events (fig. 7.1). Either way, the majority of **ROCK** is at shallow detector depths ($D_{\text{min}} < 80$ cm). The **MCNO** Depth distributions for the two flavours are similar (fig. 7.1). The **GOLD** distributions exhibit a surplus of events for $D_{\text{min}} < 80$ cm relative to **MCNO**, which is an indication of the background contamination of **GOLD**. This is the case irrespective of neutrino flavour.

The measured energy distributions for each flavour of the **GOLD**, **MCNO** and **ROCK** samples are shown in fig. 7.2. The **ROCK** distributions are sharply peaked at low energies. The **GOLD** ν_e -like data shows a small excess relative to **MCNO** around 800 MeV, but overall the background contamination of **GOLD** is not as evident in terms of energy, as it is in terms of depth.



• **Figure 7.1:** Depth distributions for ν_μ -like (left) and ν_e -like (right) GOLD, MCNO and ROCK.



• **Figure 7.2:** Energy distributions for ν_μ -like (left) and ν_e -like (right) GOLD, MCNO and ROCK.

7.1.1 Background Fits for Each Flavour Separately

The D_{\min} versus N_{Hits} space is divided into six zones, as defined in §5.6.2. The populations of the six zones for ν_e -like and ν_μ -like **GOLD**, **MCNO** and **ROCK** events are summarised in Table 7.1. As it has already been observed, the **ROCK** data heavily populates zones 1, 2 and 5 (small events near the edge), while the **GOLD** and **MCNO** data are more evenly distributed (fig. 7.3).

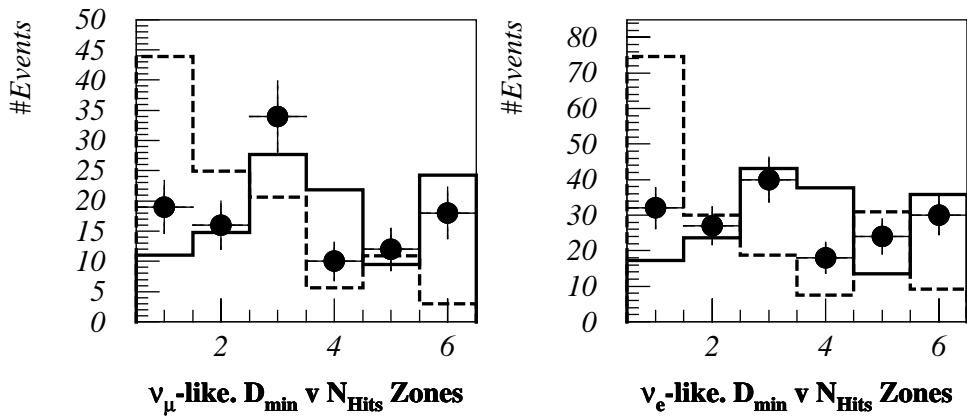
The fit is conducted as in §5.6.3. The results are summarised in Table 7.2. The contamination of **GOLD** by background for both ν_e -like and ν_μ -like data is of the order of 33%. The background fit requires a number of ν_e -like events that is within the 20% uncertainty [71] of the prediction of the absolutely normalised **MCNO**. However, the population of the ν_μ -like data is almost half that of the absolutely normalised **MCNO**. The populations of the six zones for **GOLD** and the best **MCNO+ROCK** fit are shown in fig. 7.4. The best fit does not agree well with **GOLD** in zones 3 and 4, i.e. for small and medium sized events in the heart of the detector. This may be due to either of the following reasons:

- The **ROCK** sample may not describe the background contamination in **GOLD** in every detail. This is a hard fact but there is little room for manoeuvre, because a detailed simulation of the processes contaminating the pure neutrino sample does not exist (see §5.1, the **BGD** sample).
- More importantly, however, the Monte Carlo neutrino sample may not describe the neutrino data correctly, simply because new Physics is in action.

Both reasons will be explored in the following sections. The flavour ratio of the data relative to the **MCNO** expectation will be calculated next and the prevailing question is how the background could affect it and whether neutrino mixing could account for the observed value.

Zone	Number of ν_μ -like events in each Zone			Number of ν_e -like events in each Zone		
	GOLD	MCNO	ROCK	GOLD	MCNO	ROCK
1	19	1757	132	32	1605	179
2	16	2354	75	27	2200	72
3	34	4408	62	40	4022	45
4	10	3471	17	18	3500	18
5	12	1505	33	24	1256	74
6	18	3858	9	30	3332	22
Total	109	17353	328	171	15915	410

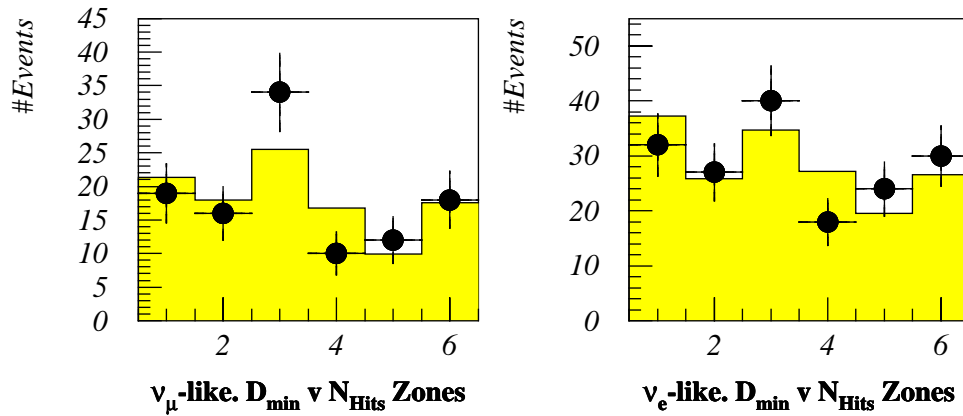
• **Table 7.1:** Populations of the six zones of the D_{\min} versus N_{Hits} space for ν_μ -like and ν_e -like GOLD, MCNO and ROCK data.



• **Figure 7.3:** Graphical representation of the population of the six zones of the D_{\min} versus N_{Hits} space for ν_μ -like and ν_e -like GOLD (error bars), MCNO (solid line) and ROCK (dashed line). MCNO and ROCK are normalised to GOLD.

	ν_μ -like	ν_e -like
a	0.687 ± 0.124	0.652 ± 0.092
x	0.313 ± 0.111	0.348 ± 0.084
Number of Neutrinos in GOLD = $280 \times a$	74.9 ± 13.5	111.5 ± 15.7
Number of MCNO Neutrinos Expected	$150.0 (\pm 20\%)$	$137.6 (\pm 20\%)$
Number of Background in GOLD = $280 \times x$	34.1 ± 12.1	59.5 ± 14.4

• **Table 7.2:** Results of background fit for each flavour separately. The MCNO expectation is normalised to the exposure of the experiment.



• **Figure 7.4:** Graphical representation of the population of the six zones of the D_{\min} versus N_{Hits} space for ν_μ -like and ν_e -like GOLD (error bars) and MCNO+ROCK best fit (shaded area).

7.1.2 The Ratio of Ratios

The Ratio of Ratios, R , as defined in Eq. 7.1, may now be calculated. There are:

- **DATA** neutrino candidates: 74.9 ± 13.5 ν_μ -like and 111.5 ± 15.7 ν_e -like events.
- **MCNO** neutrino candidates: 17353 ± 132 ν_μ -like and 15915 ± 126 ν_e -like events.

The errors on the **MCNO** event counts are statistical. The **MCNO** fractional errors are negligible compared to the **DATA** errors. The Ratio of Ratios is:

$$R = 0.62 \pm 0.14(\text{stat.}) \pm 0.05(\text{syst.}).$$

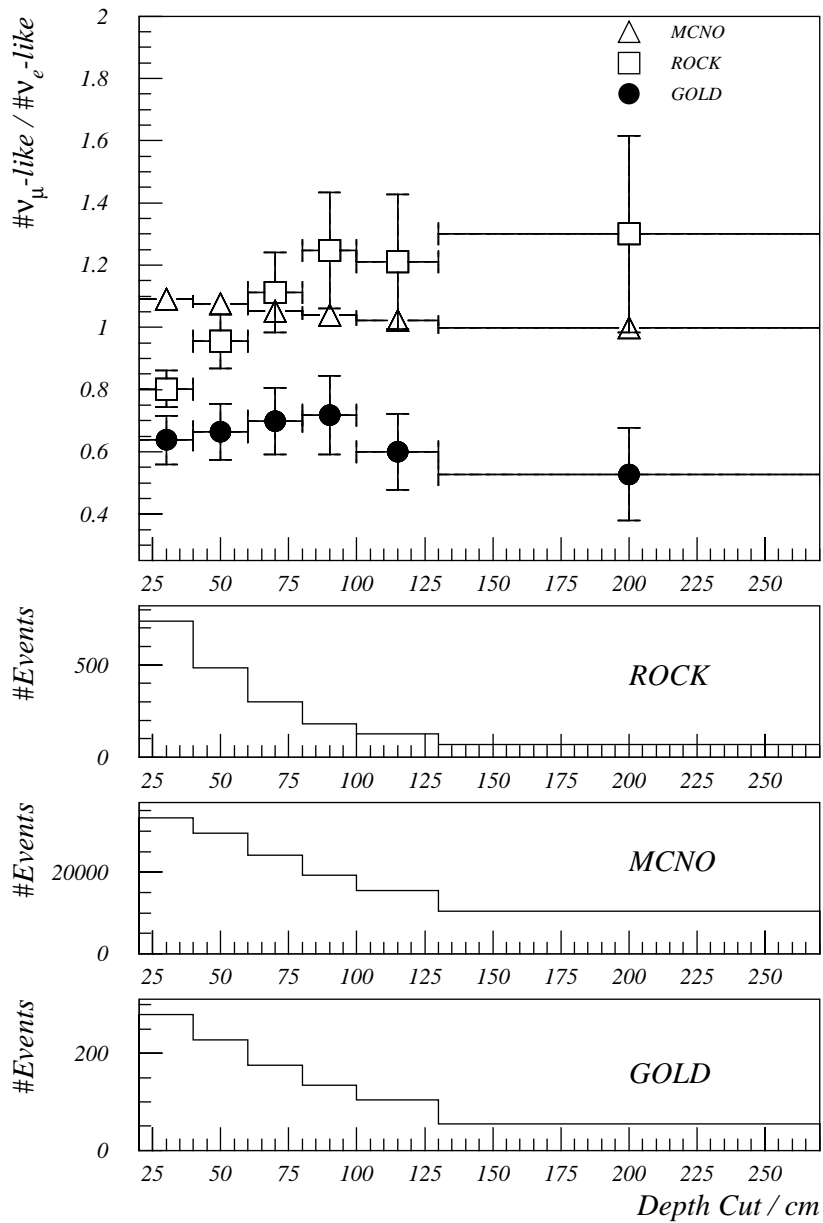
The statistical error is the sum in quadrature of the errors of the data neutrino candidates and includes the error due to the background correction. The systematic error is due to a variety of sources, mainly due to known Monte Carlo short-comings (including uncertainties in the neutrino flux and cross-sections), and has been calculated to be of the order of 8% [47].

The above result agrees very well with the recent value of R quoted by the scanning Soudan 2 team; it also agrees well with the water Čerenkov experiments (Table 2.2). This is very important because these results refer to different quantities. The present analysis uses all the contained data in Soudan 2, including neutral current and inelastic (multi-prong) processes. The Soudan 2 scanning team has produced a value of R using only the single-prong events, the flavour of which can typically be identified by eye. Most of them were quasi-elastic charged current interactions with a visible (and in most cases correctly identified) lepton; identified recoil protons were also allowed. Moreover, the scanned analysis has a larger exposure (by ≈ 0.5 fiducial kTonYear) because it includes the data from the early days of the experiment. The scanned single-prong event sample used in the measurement of R comprises 228 events. For the calculation of R , only 124 events are common between the present analysis and the scanned analysis [44]. Similarly to the Soudan 2 scanned analysis, the Kamiokande, Super-K and IMB groups use the quasi-elastic interactions in their Sub-GeV single-ring analyses.

7.1.3 Discussion on R: the Background Hypothesis

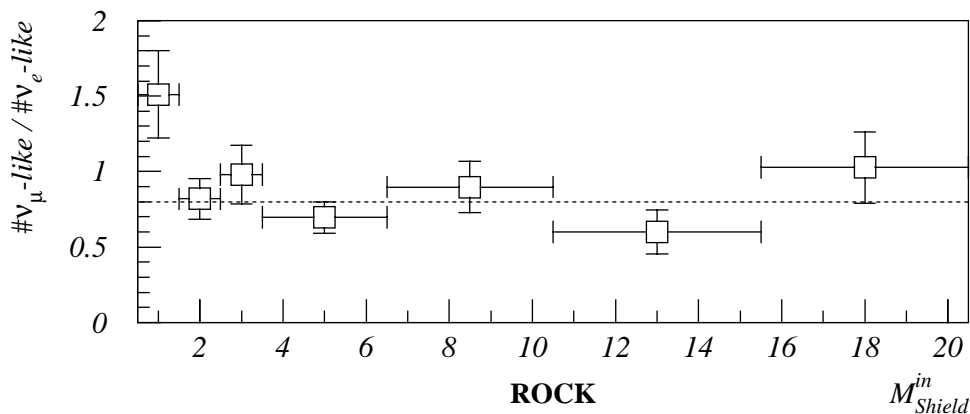
A much discussed issue is the contamination of the contained event sample from neutral particles that enter the main detector undetected by the shield. Ryazhskaya claimed that the atmospheric neutrino anomaly could be accounted for by interactions of CR-muons in the rock surrounding the experimental hall producing a high yield of π^0 particles, the products of which, upon entering the main detector, produce events with a track to shower ratio of 1 to 5 [56] [73]. If these allegations were correct, the background sample would exhibit such a low track to shower ratio. However, the Soudan 2 fully scanned analysis found a ratio of tracks to showers in their background sample of 1.2:1 [45], while the Kamiokande Collaboration published a uniform spatial distribution for their contained events, which would not have been the case if they had been dominated by background [42].

In the present analysis, the flavour ratio of ν_μ -like to ν_e -like events is 0.80 ± 0.06 for **ROCK**, 1.09 ± 0.01 for **MCNO** and 0.64 ± 0.08 for **GOLD** (derived from Table 7.1). The variation of the flavour ratio in each sample as a function of a depth cut (i.e. of a fiducial volume cut) is illustrated in fig. 7.5. In **ROCK**, the pattern observed is as expected from the individual depth distributions. In shallow depths (below 70 cm), the ν_e -like events are relatively abundant because most of the electromagnetic radiation will have interacted by that depth (the radiation length in Soudan 2 is ≈ 15 cm). For depths above 70 cm **ROCK** interactions are mainly induced by neutrons and the ν_μ -like to ν_e -like ratio increases to approximately 1.3, albeit with large errors because of low statistics. In **MCNO** the flavour ratio is flat and approximately equal to unity as a function of the depth cut. Similarly, the **GOLD** flavour ratio is constant as a function of depth and is consistently lower to the other two for all depths. This implies that no linear combination of **MCNO** and **ROCK** can reproduce the **GOLD** sample



• **Figure 7.5:** Flavour Ratio of ν_{μ} -like to ν_e -like events in **ROCK**, **MCNO** and **GOLD** as a function of depth (fiducial volume) cut in the detector (top) (derived from fig. 7.1): each bin contains the flavour ratio for events that are within that depth. The **ROCK**, **MCNO** and **GOLD** cumulative Depth distributions for both flavours together are shown at the bottom. The first bin (starting at 20 cm) includes all events.

Additional information on the flavour content of the true background sample can be extracted from the **ROCK** sample. The dependence of the flavour ratio on the shield multiplicity in the T_0 -window is flat (fig. 7.6). This justifies the extrapolation of the **ROCK** flavour ratio to the zero-shield true background sample and reinforces the assumption that **ROCK** describes the true background correctly. For the sake of completeness, fig. 7.6 includes the flavour ratio of the **BGD** sub-set of unit-shield-multiplicity that has been excluded from **ROCK** on the grounds that it is contaminated by true neutrino interactions. It is observed that the flavour ratio unit-shield-multiplicity is high, in contradiction to the expectation since the gold flavour ratio is low. However, neutrino events that have unit-shield-multiplicity are usually small, single-loom events with a wide T_0 -window. Single-loom track events will typically have a wider T_0 -window than single loom shower events because the latter occupy more volume for the same event length. Therefore, there is a greater chance for small neutrino tracks to be vetoed by random shield hits than there is for small neutrino showers, which explains the high flavour ratio for unit-shield-multiplicity events.



• **Figure 7.6:** Flavour ratio of ν_μ -like to ν_e -like events in **ROCK** as a function of the shield multiplicity in the T_0 -window. The last bin contains all events with shield multiplicity above or equal to 16.

In conclusion, it is believed that **ROCK** describes the flavour ratio of true (zero-shield) background correctly. It is also observed that **GOLD** may not be described as a linear combination of **MCNO** plus **ROCK**, i.e. *the observed neutrino flavour anomaly cannot be attributed to background contamination of the GOLD sample.*

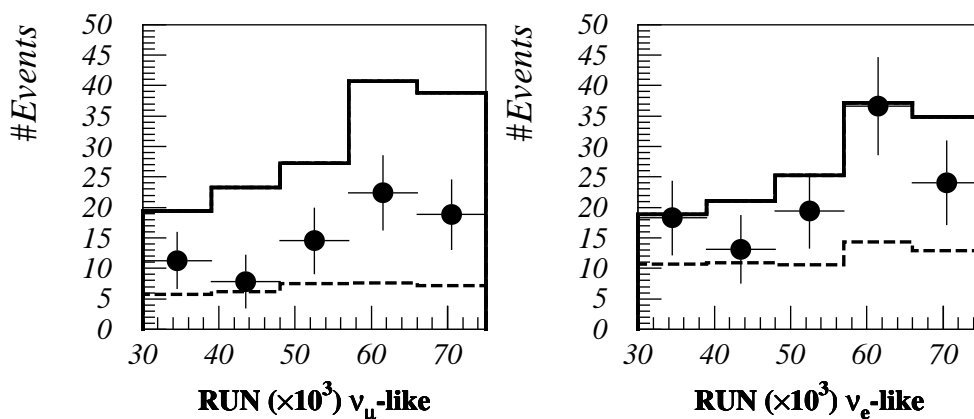
7.1.4 Further Investigation of the Anomaly

In this section the run-number and the flavour and zenith angle distributions of ν_e -like and ν_μ -like neutrino data will be compared to the **MCNO** expectation. The neutrino distributions will be extracted from the **GOLD** data by subtracting the relevant amount of **ROCK**, as determined by the background fit. The **MCNO** distributions will be normalised according to the number of neutrino events expected by the exposure of the experiment.

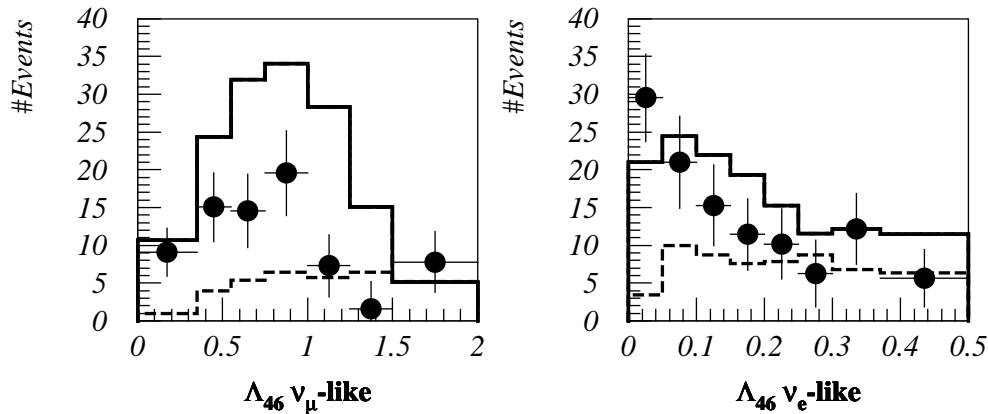
• Run Number Distributions

The distributions of run number for ν_e -like and ν_μ -like data are presented in fig. 7.7. Two points are worthy of attention:

- The ratio of observed-to-expected ν_μ -like events is constant and equal to



• **Figure 7.7:** Distribution of Run number for ν_μ -like events (left) and ν_e -like events (right): (i) **GOLD** data, where the amount of **ROCK** calculated in background fit has been subtracted (error bars); (ii) **MCNO**, absolutely normalised (solid line); (iii) **ROCK**, normalised to the amount of background calculated in the fit (dashed line).



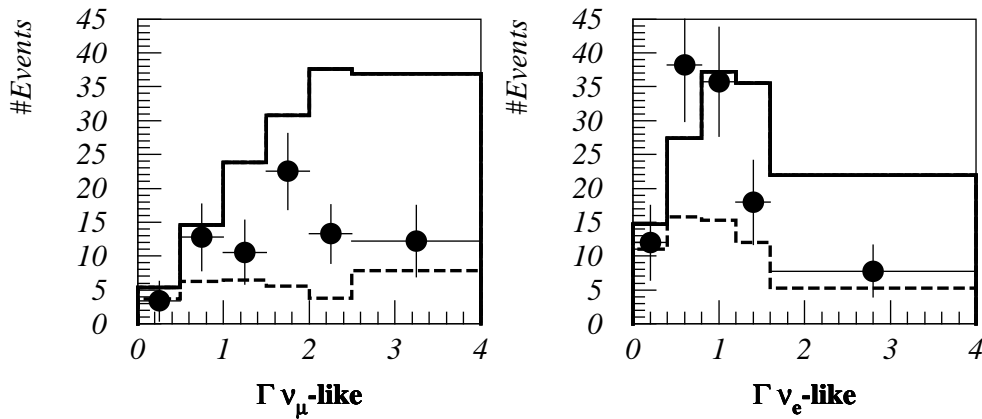
• **Figure 7.8:** Distribution of Λ_{46} for ν_{μ} -like events (left) and ν_e -like events (right): (i) **GOLD** data, where the amount of **ROCK** calculated in background fit has been subtracted (error bars); (ii) **MCNO**, absolutely normalised (solid line); (iii) **ROCK**, normalised to the amount of background calculated in the fit (dashed line). Notice the different abscissa scales.

approximately 2 throughout the period of data collection analysed in the present thesis. The ν_e -like distribution is slightly lower but overall in agreement with the expected flux when the 20% uncertainty in the absolute normalisation is considered. In general, the shape of the data distributions follows that of the expectation.

- The ratio of neutrino signal-to-background is higher for the recent data than it is for the earlier data. This is due to two reasons: (i) the detector has been growing in size over time and (ii) the background rejection has improved with both the main detector and the shield becoming more efficient.

• Λ_{46} Distributions

The deficit of ν_{μ} -like events is apparent in the distributions of Λ_{46} for **GOLD** minus **ROCK** (where the normalisation of **ROCK** is determined from the background fit) compared to the absolutely normalised **MCNO** sample (fig. 7.8). The data deficit is very pronounced for very linear events ($\Lambda_{46} > 1.0$). For ν_e -like events **GOLD** minus **ROCK** agrees with the absolutely



• **Figure 7.9:** Distribution of Γ for ν_μ -like events (left) and ν_e -like events (right): (i) **GOLD** data, where the amount of **ROCK** calculated in background fit has been subtracted (error bars); (ii) **MCNO**, absolutely normalised (solid line); (iii) **ROCK**, normalised to the amount of background calculated in the fit (dashed line).

normalised **MCNO**, in particular when the 20% normalisation uncertainty in the latter is taken into account [71].

• Γ Distributions

The second flavour estimator, Γ , is less powerful than Λ_{46} . It will be used here in order to qualitatively check the results obtained by Λ_{46} .

The Γ distributions for ν_e -like and ν_μ -like events are shown in fig. 7.9. The ν_μ -like data exhibits a deficit relative to the absolutely normalised **MCNO** sample for $\Gamma > 2.0$, which corresponds to linear events. This is similar to what has been observed with Λ_{46} and could be accounted for by $\nu_\mu \leftrightarrow \nu_\tau$ mixing.

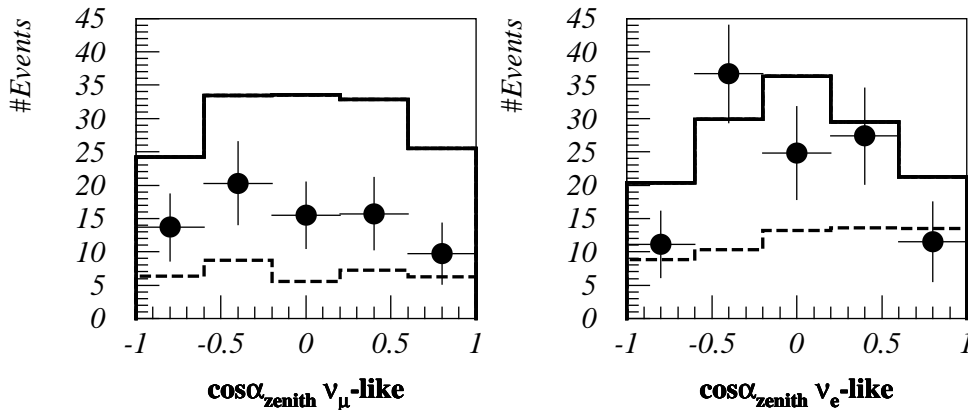
The ν_e -like data exhibits large discrepancies relative to **MCNO** in the shape of the Γ distributions: the data is considerably more spherical than the **MCNO** expectation, an observation which cannot be explained in terms of neutrino mixing. It is possible that there is an unknown systematic effect between real data and **MC** that affects Γ . Such a systematic effect may be attributed to the lack of simulation of the de-excitation of final state nuclei in the Soudan 2 Monte Carlo (§4.1). The low-energy products of nuclear de-excitation would

interact with the detector medium and deposit ionisation isotropically around the event vertex. By definition, Γ is sensitive to such outlying hits, because its calculation involves the second moments of hits about the event axis (§6.1.2). The absence of such hits in the MC simulation would make the MC sample look more linear when examined with Γ . However, this effect is expected to diminish with increasing energy because the contribution of an additional 3D hit is larger the smaller the original number of 3D hits is. It is also expected to affect events of both flavours. Because of the above uncertainties, Γ is not used any further.

- **Zenith Angle and L/E _{ν} Distributions**

The zenith angle distributions are of interest because they could offer a strong signature on neutrino mixing. For example, if ν_μ mix with ν_τ with a large value of $\sin^2 2\theta$ and $\Delta m^2 \approx 10^{-2} \text{ eV}^2$, then the ν_μ events coming from the other side of the Earth would oscillate. This would result in a deficit of muon neutrinos coming from the antipodes relative to those coming from right above the detector, which would be evident in the zenith angle distribution for the data. However, the neutrino direction estimator (§6.4) is ambiguous in determining the sense of travel of quasi-elastic muon neutrino interactions. It is therefore expected that if neutrinos do oscillate in the $\nu_\mu \leftrightarrow \nu_\tau$ mode, then the apparent zenith angle deficit for down-coming ν_μ -like events will be significantly reduced.

The MCNO distributions for both flavours exhibit larger neutrino flux near the horizontal ($\cos \alpha_{zenith} = 0$), fig. 7.10. This pattern is also observed in the data and is due to (i) the detector acceptance and (ii) the larger distance atmospheric muons travel in that direction, which increases the chance that they decay and produce an electron and muon neutrino pair. The deficit in the ν_μ -like events is uniform as a function of the zenith angle, an observation that can be accounted for by neutrino mixing with a large value of Δm^2 so that neutrinos from all directions have oscillated before interacting in the detector. Finally, in the ROCK sample, the ν_e -like zenith angle distribution shows a preference for down-going events, as expected, because these events are induced by down-going CR-muon interactions in the rock surrounding the detector.



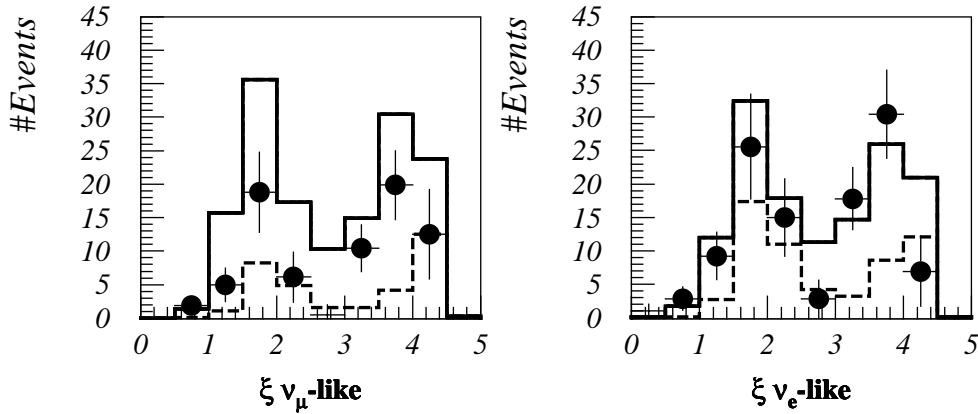
• **Figure 7.10:** Distribution of the cosine of the zenith angle for ν_μ -like events (left) and ν_e -like events (right): (i) **GOLD** data, where the amount of **ROCK** calculated in background fit has been subtracted (error bars); (ii) **MCNO**, absolutely normalised (solid line); (iii) **ROCK**, normalised to the amount of background calculated in the fit (dashed line).

As expected from the zenith angle distributions, the ν_μ -like data shows a homogeneous deficit across the measured L/E_ν spectrum (fig. 7.11, using estimator ξ , see §6.5). The deficit is larger for $L/E_\nu < 10^3$ km/GeV, i.e. in the opposite sense than it is expected for muon neutrinos oscillating, but the effect is not significant. The ν_e -like distribution generally agrees with the Standard Model expectation.

• Zenith Angle Distributions after a Low Energy Cut

The application of a low energy cut, which is defined by rejecting events with fewer than 40 3D hits (≈ 850 MeV), is beneficial to the performance of both flavour and direction estimators, as discussed in §6.1 and §6.4. Moreover, the background contamination of **GOLD** is significantly reduced; it is estimated to be below 10% (§5.6.4) and will be neglected in the discussion that follows in this section.

The zenith angle distributions for **GOLD** ν_e -like and ν_μ -like events after the application of the low energy cut is shown in fig. 7.12. The distributions have three bins only because of limited statistics in this high energy regime. If neutrino mixing in the $\nu_\mu \leftrightarrow \nu_\tau$ mode were the case, we would expect a deficit in the up-going ν_μ -like events.



• **Figure 7.11:** Distribution of the L/E_ν estimator, ξ , for ν_μ -like events (left) and ν_e -like events (right): (i) **GOLD** data, where the amount of **ROCK** calculated in background fit has been subtracted (error bars); (ii) **MCNO**, absolutely normalised (solid line); (iii) **ROCK**, normalised to the amount of background calculated in the fit (dashed line).

This is not observed. In fact, the data has the opposite tendency, but the statistical significance of the observation is poor. The ν_e -like data presents the familiar increase in the number of events in the horizontal bin.

We may go one step further and invert these distributions for true flavour by using the flavour misidentification matrix for events of 40 or more 3D hits, as calculated for the $\Lambda_{46}-N_{\text{Hits}}$ cut in Table 6.4. For each bin (up-, horizontal- or down-going), the number of ν_e -like and ν_μ -like events is inverted to obtain the data true- ν_e and true- ν_μ zenith angle distributions. The trend for the ν_μ -data to show a relative deficit of down-going events persists, but is not any more significant. The ν_e distribution is largely unchanged.

Finally, we may also invert each of the true ν_e and ν_μ data zenith angle distributions for true direction. Since the muon sense of direction is largely ambiguous, this enhances the deficit of down-going muons. The direction misidentification matrices for true- ν_e and true- ν_μ MCNO data for events with 40 or more 3D hits are given in Tables 7.3 and 7.4. The statistical errors of the matrix elements are very small because of the very large MCNO sample. It is observed that the diagonal elements of the ν_e matrix are larger than

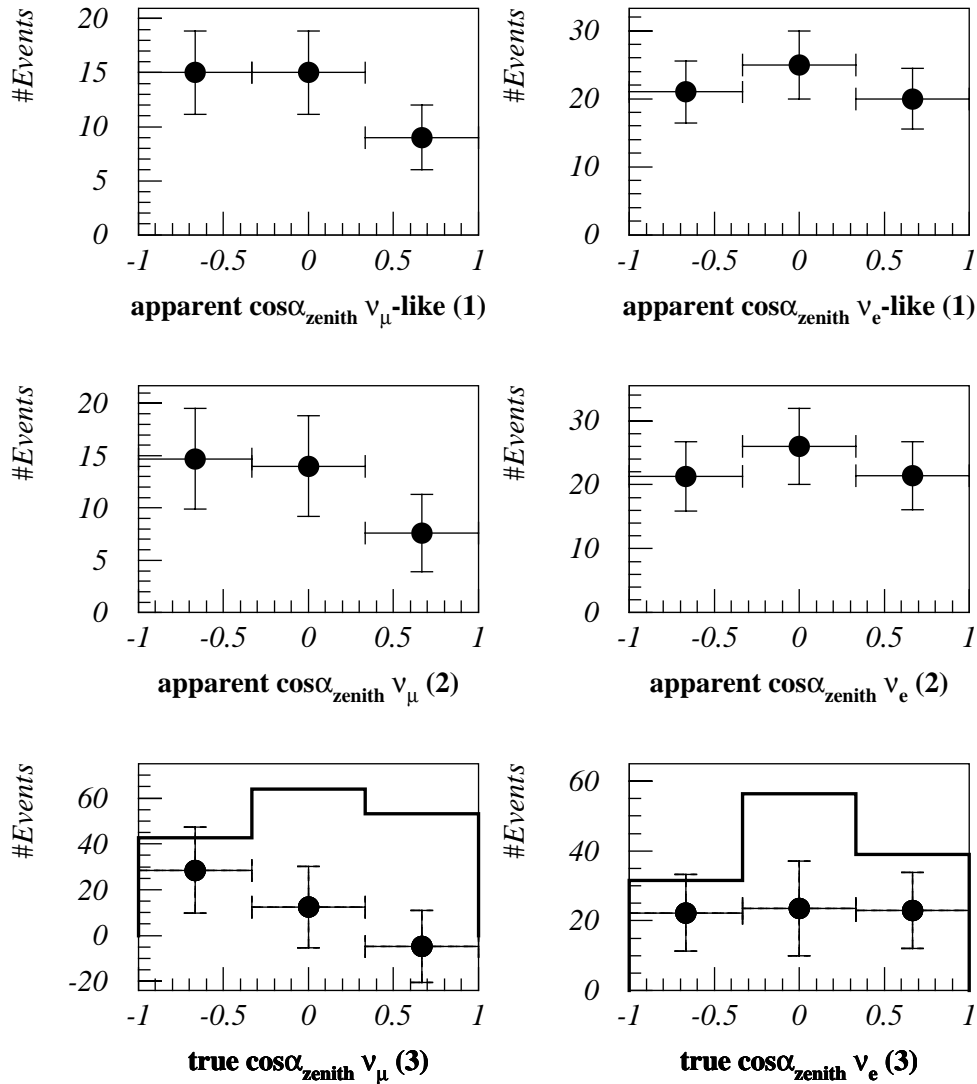
those of the ν_μ matrix, as it is discussed in §6.4. After inverting for true neutrino direction we see that the data is consistent with no down-going ν_μ events at all. The error bars are very large however, and, interesting as this result may be, it is not significant. Beware, the errors are correlated. The true ν_μ zenith angle distribution is consistent with a uniform distribution, as is the case for the true ν_e zenith angle distribution.

Electron neutrinos	MCNO measured neutrino direction			
MCNO true neutrino direction		Up	Horizontal	Down
	Up	0.605	0.253	0.142
	Horizontal	0.196	0.613	0.191
	Down	0.141	0.260	0.599

• **Table 7.3:** Direction misidentification matrix for true- ν_e MCNO data with 40 or more 3D hits.

Muon neutrinos	MCNO measured neutrino direction			
MCNO true neutrino direction		Up	Horizontal	Down
	Up	0.451	0.312	0.237
	Horizontal	0.240	0.526	0.234
	Down	0.245	0.313	0.442

• **Table 7.4:** Direction misidentification matrix for true- ν_μ MCNO data with 40 or more 3D hits.



• **Figure 7.12:** Distribution of the cosine of the zenith angle for ν_μ -like events (left) and ν_e -like events (right) after applying a 40-hit cut (1, top); similarly, after inverting for true flavour in each zenith angle bin (2, middle); similarly, after inverting for true neutrino direction (3, bottom). For the third case the true MCNO ν_μ and ν_e zenith angle absolutely normalised distributions are also shown.

7.2 A Multi-Variable Fit

An alternative approach to establish the atmospheric neutrino anomaly is by means of a multi-variable fit that is conducted on the complete data set and not each flavour separately. The **GOLD** data is fitted to a sample comprised of a number of A_{NO} **MCNO** events and a number of X_{NO} **ROCK** events, where A_{NO} and X_{NO} are the parameters of the fit. This treats the presence of background in **GOLD** properly. The mechanism of the fit is described in Appendix B. The fit is sensitive to the following variables:

- Flavour: the data is divided into ν_e -like and ν_μ -like events. This is achieved by means of the Λ_{46} - N_{Hits} cut defined in §6.2.
- Neutrino energy: this is a partial requirement for knowing the neutrino L/E_ν phase. It will also help in the separation of the neutrino signal from background. This is achieved in terms of the energy estimator, E_ν^{meas} , defined in §6.3.
- Neutrino direction: this, together with E_ν^{meas} , discriminates events according to the neutrino L/E_ν phase. The direction estimator is used (§6.4).
- Event depth: this is a requirement for the efficient separation of background from neutrino data. It is achieved in terms of the depth estimator, D_{min} , described in §5.3.2.

The function that is used in the fit is a 4-dimensional distribution of the flavour, energy, direction and depth estimators. The bin divisions of this 4-D distribution are optimised such that **MC** and **ROCK** reasonably populate each bin; a compromise is reached, of course, since these two samples have very different characteristics, in particular in terms of depth. It has also been chosen to have the minimum possible number of bins so that we would not be overly concerned with finite **MC** and **ROCK** statistics. In any case, the **GOLD** data statistics are the smallest and dominate the statistical errors. The total number of bins in the 4-D distribution is 24 and breaks down as follows:

A_{NO}	221.9 ± 26.9
X_{NO}	62.6 ± 21.3
χ^2/ndf	42.53 / 22
χ^2 probability	5.4×10^{-3}

• **Table 7.5:** Results of multi-variable no-oscillations plus background fit to the **GOLD** data.

- 2 Flavour bins dividing the data into ν_e -like and ν_μ -like events by means of the Λ_{46} - N_{Hits} flavour cut.
- 2 Energy bins, dividing the data at $E_\nu^{\text{meas}} \approx 675 \text{ MeV}$.
- 3 cosine of the Zenith angle bins, dividing the data into up-going, horizontal-going and down-going events.
- 2 Depth bins, dividing the data at 60 cm.

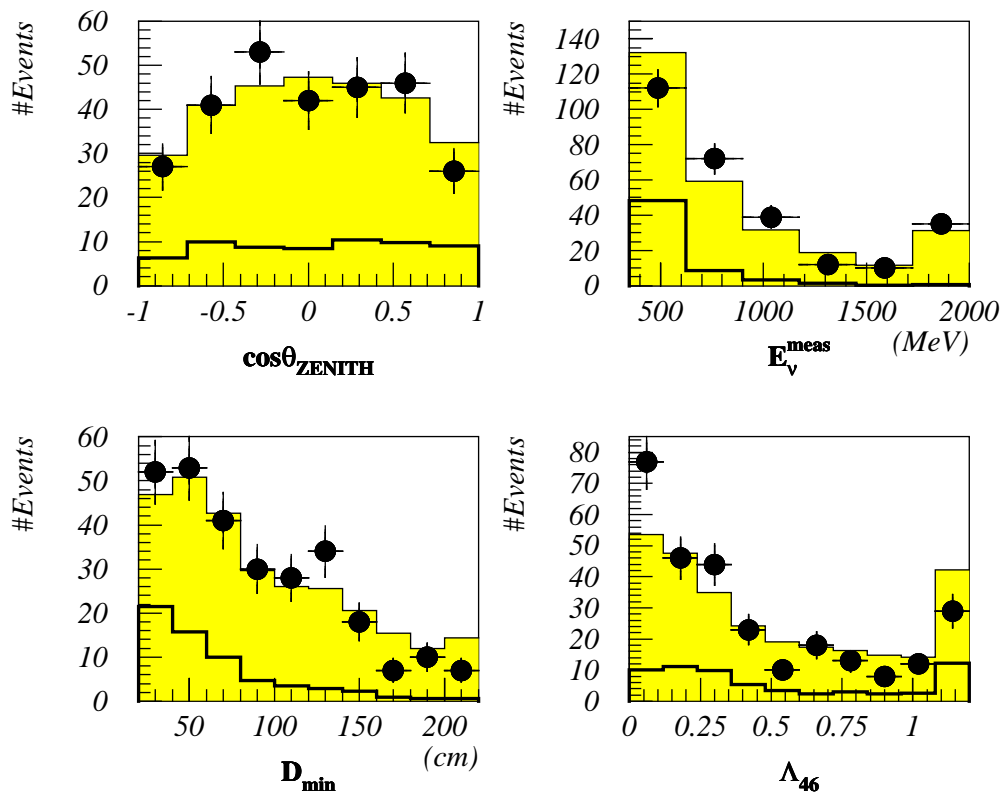
7.2.1 Data Compared to No Oscillations Model

The results of the fit are summarised in Table 7.5. The background contamination in **GOLD** is now calculated to be $(22 \pm 7)\%$. This figure is in agreement with the background estimate from the depth-energy fit, as conducted in the previous section, which concluded that about a third of the population of the **GOLD** sample is attributed to background.

The **GOLD** data is compared to the best fit of **MCNO** plus **ROCK** by means of a χ^2 -test over the 24 bins of the multi-variable surface, as described in Appendix B. The quality of the fit is poor: the χ^2 probability is very low (5.4×10^{-3}) which implies that *the model does not describe the data*.

Distributions of the quantities fitted are shown for the data against the best fit **MCNO** plus **ROCK** model (fig. 7.13). The number of bins in each of the flavour, energy, zenith angle and depth estimators is larger than that used in the fit. It is observed that the

flavour content of the data is badly described by the model. In particular, the model predicts more muon-like events (at high values of Λ_{46}) and less electron-like events (at low values of Λ_{46}) than are observed in the GOLD data. The energy, zenith angle and depth distributions for the model do not show large discrepancies when compared to the data. Note that the energy distributions suggest that the background population in the model is too high. More on the subject follows in the next section.



• **Figure 7.13:** Distributions of zenith angle, neutrino energy, depth and Λ_{46} flavour estimators for (i) the GOLD data (error bars), (ii) best fit MCNO plus ROCK model (shaded area) and (iii) ROCK, normalised to multi-variable fit solution (solid line).

7.3 Neutrino Mixing Searches

In this section it will be assumed that neutrino mixing is the physical explanation for the observed atmospheric neutrino anomaly. Under a mixing mode hypothesis, a log-likelihood fit to the data is conducted in order to determine the preferred neutrino mixing parameters. The process is performed for the $\nu_\mu \leftrightarrow \nu_e$, $\nu_\mu \leftrightarrow \nu_\tau$ and 3-generation maximal mixing hypotheses.

The **GOLD** data is compared with the sum of MC-simulated atmospheric neutrino data and background, using the multi-variable fit (as described in the section above) at *each point of the neutrino mixing parameter space*. The **MCAF** neutrino sample (§4.3) will be used to define the MC distributions, while the background contamination of **GOLD** is described by the **ROCK** event sample. The fitted MC and **ROCK** populations, $A(\alpha)$ and $X(\alpha)$, are a function of the mixing parameters, denoted here by α . For each set of mixing parameters the fit will maximise the log-likelihood of the experiment as a function of $A(\alpha)$ and $X(\alpha)$. The quality of the log-likelihood fit is determined by both a χ^2 -test and the estimation of the likelihood of the log-likelihood, as described in Appendix B.

7.3.1 Oscillations Mode: $\nu_\mu \leftrightarrow \nu_\tau$

The data is fitted for neutrino mixing in the $\nu_\mu \leftrightarrow \nu_\tau$ mode. The results are summarised in Table 7.6. The $\text{MC}(\nu_\mu \leftrightarrow \nu_\tau)$ normalisation obtained by the fit is in good agreement with the expectation from the exposure of the experiment. The exclusion regions for different confidence levels are shown in fig. 7.14. The data prefers large values of $\sin^2 2\theta$; $\Delta m^2 > 4 \times 10^{-3} \text{ eV}^2$ for $\sin^2 2\theta = 1$ at 90% confidence level. The variation of log-likelihood as a function of Δm^2 for $\sin^2 2\theta = 1$ shows there is little power for resolving Δm^2 above 10^{-2} eV^2 (fig. 7.15).

The model generally describes the data well (fig. 7.16). The zenith angle distribution is flat, which is why Δm^2 is not constrained from the top. The model energy distribution exhibits a small excess below 600 MeV, which is where the vast majority of

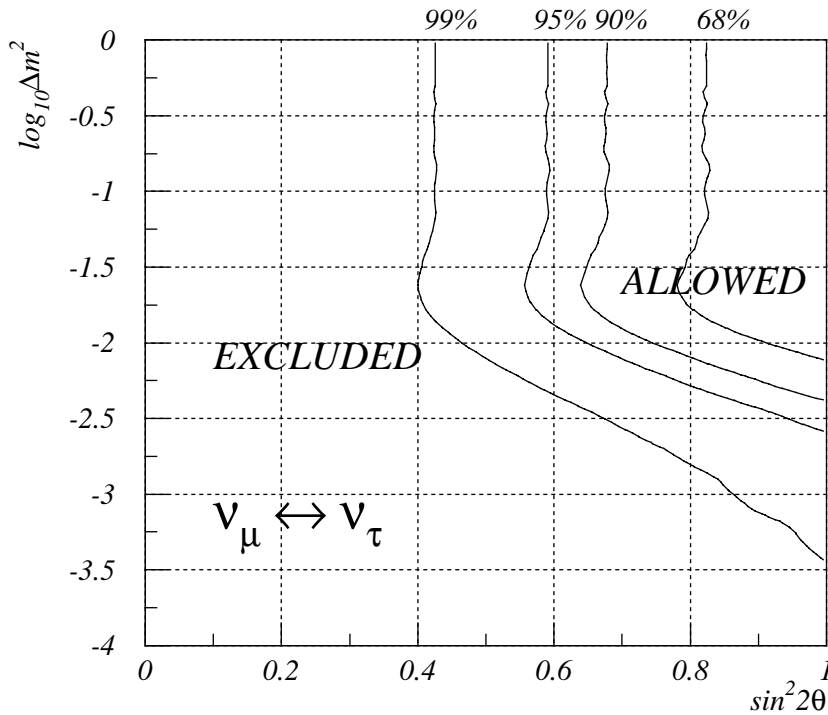
Maximum of log-likelihood at	$\sin^2 2\theta = 1, \Delta m^2 = 0.024 \text{ eV}^2$
MC population at maximum: $A(\mu \leftrightarrow \tau)$	222.5 ± 25.3
MC population expected at maximum	$214.9 (\pm 20\%)$
ROCK population at maximum: $X(\mu \leftrightarrow \tau)$	56.6 ± 20.5
Value of log-likelihood at maximum	-62.24
Log-likelihood probability	30.4%
χ^2/ndf	$23.27 / 20$
χ^2 probability	27.6%

• **Table 7.6:** Results of $\nu_\mu \leftrightarrow \nu_\tau$ mixing multi-variable fit with background.

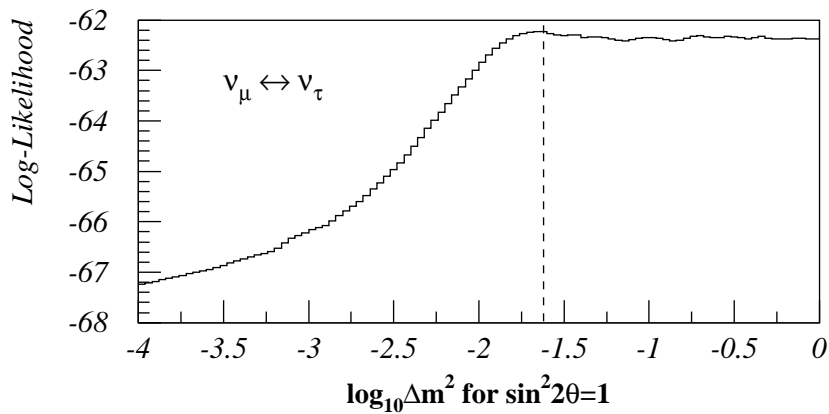
background events lie. Given that the error on the background count is above 30% (Table 7.6), the model is not in disagreement with the data. The model agrees with the data in terms of Λ_{46} , which was not the case for the no-oscillations hypothesis, discussed in the previous section. In the depth distribution, the small deficit of events deep in the detector (above 150 cm) cannot be accounted for by the model. The presence of background at this depth is very small and the large error on the background normalisation cannot cover the discrepancy. Nevertheless, statistics are poor in the region and the observation may not prove significant after the collection of more data. However, if this effect persists, the neutrino oscillations hypothesis may prove unsuitable to describe the data.

The quality of the fit is good: the χ^2 probability (Appendix B) is 27.6%. A similar answer is obtained from the distribution of expected maximum log-likelihood values, obtained by simulating 1000 MC experiments with background at the solution point (Appendix B). There are 304 simulated experiments with log-likelihood below -62.25 (fig. 7.17).¹⁶ Hence, if the truth was at the point where the log-likelihood is maximised for the data, the probability of obtaining a value of log-likelihood of -62.25 or less is 30.4%.

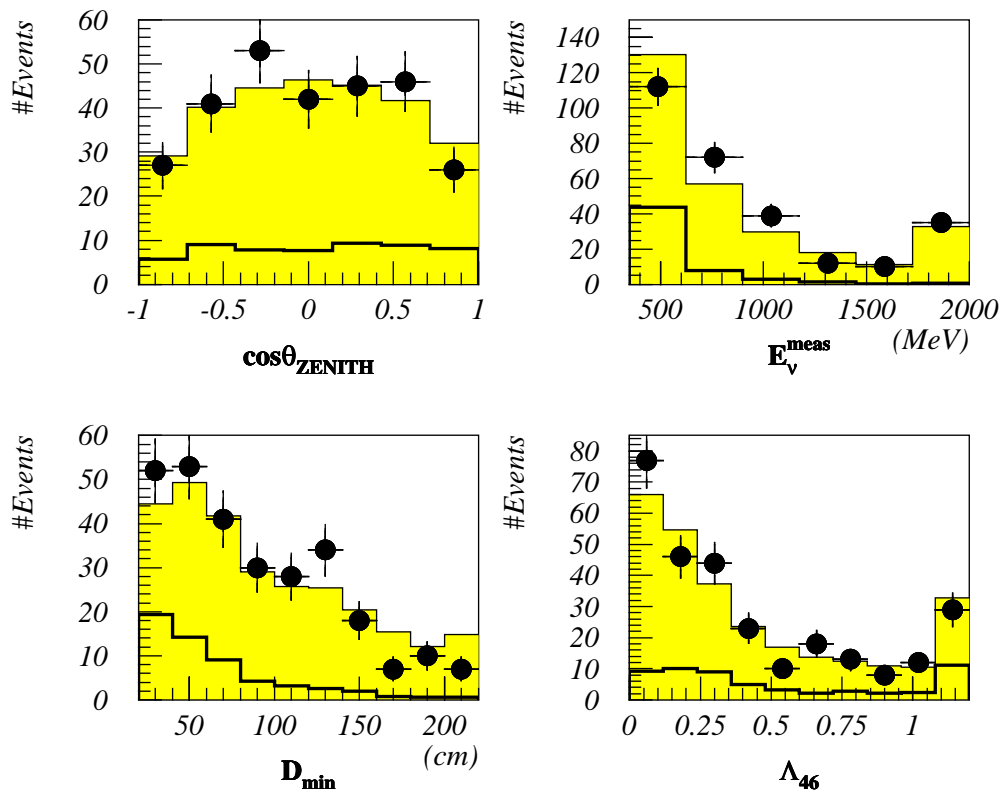
¹⁶ The bin width of the log-likelihood distribution is quarter of a unit and an approximation is necessary: the value of -62.25 is the closest to the maximum log-likelihood of -62.23 obtained by fitting the data.



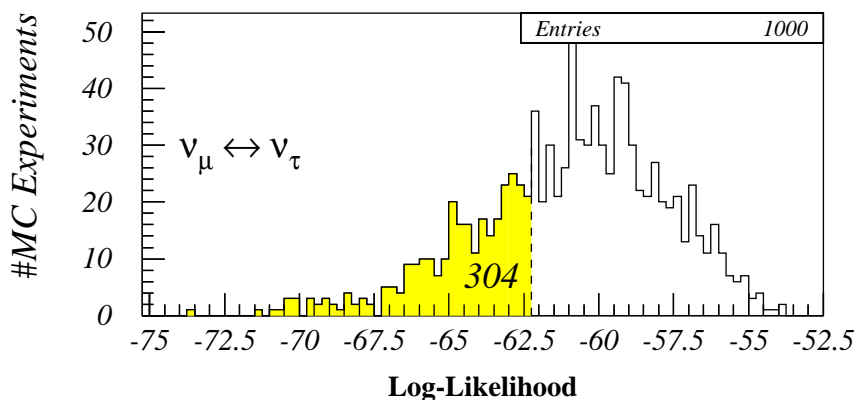
• **Figure 7.14:** Neutrino mixing parameters, Δm^2 and $\sin^2 2\theta$, limits for $\nu_\mu \leftrightarrow \nu_\tau$ oscillations mode, as determined by log-likelihood multi-variable fit. The 68%, 90%, 95% and 99% confidence level limits are shown.



• **Figure 7.15:** Variation of log-likelihood as a function of Δm^2 for $\sin^2 2\theta = 1$ and $\nu_\mu \leftrightarrow \nu_\tau$ mixing. The best fit (maximum) at $\Delta m^2 = 0.024 \text{ eV}^2$ is indicated.



• **Figure 7.16:** Distributions of zenith angle, neutrino energy, depth and Λ_{46} flavour estimators for (i) GOLD data (error bars), (ii) best fit MC($\nu_{\mu} \leftrightarrow \nu_{\tau}$) plus ROCK model (shaded area) and (iii) ROCK, normalised to multi-variable fit solution (solid line).



• **Figure 7.17:** Distribution of expected log-likelihood at the maximum of the Δm^2 and $\sin^2 2\theta$ neutrino mixing parameter space. It has been obtained by fitting 1000 MC experiments whose truth is at the $\nu_{\mu} \leftrightarrow \nu_{\tau}$ solution of the data fit. Background has been added to each of these experiments – see Appendix B.

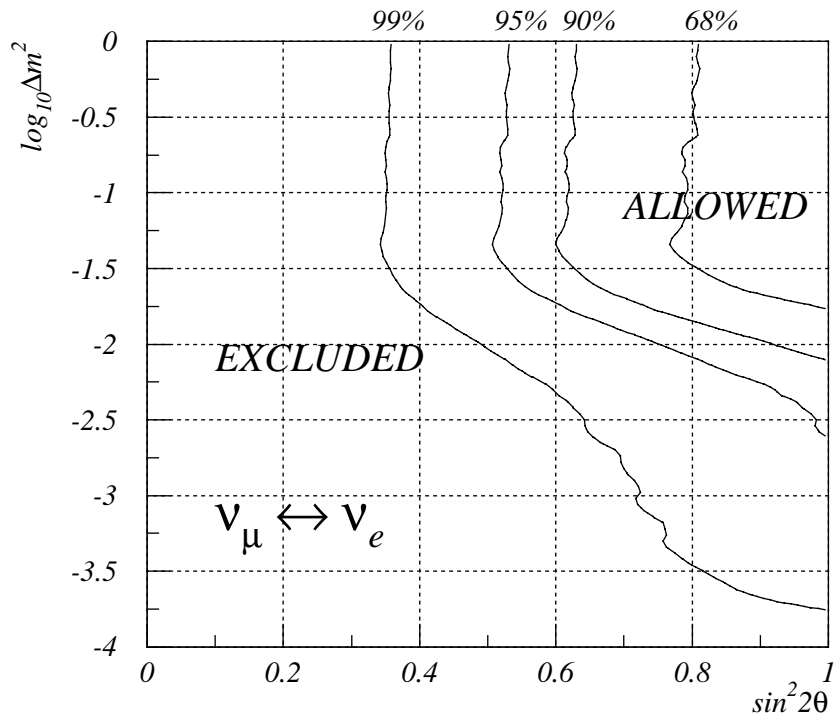
7.3.2 Oscillations Mode: $\nu_\mu \leftrightarrow \nu_e$

The data is fitted for neutrino mixing in the $\nu_\mu \leftrightarrow \nu_e$ mode. The results are summarised in Table 7.7. The $\text{MC}(\nu_\mu \leftrightarrow \nu_e)$ normalisation expected by the exposure of the experiment is high compared to the number of neutrinos determined by the fit in the data. The exclusion regions for different confidence levels are shown in fig. 7.18. The data prefers large values of $\sin^2 2\theta$; $\Delta m^2 > 6 \times 10^{-3} \text{ eV}^2$ for $\sin^2 2\theta = 1$ at 90% confidence level. Similarly to the $\nu_\mu \leftrightarrow \nu_\tau$ mode there is no upper constraint for Δm^2 (fig. 7.19). The data cannot discriminate between $\nu_\mu \leftrightarrow \nu_e$ and $\nu_\mu \leftrightarrow \nu_\tau$ neutrino mixing: the distributions of zenith angle, energy, depth and flavour estimators are very similar between the two models (fig. 7.20 for $\nu_\mu \leftrightarrow \nu_e$ and fig. 7.16 for $\nu_\mu \leftrightarrow \nu_\tau$).

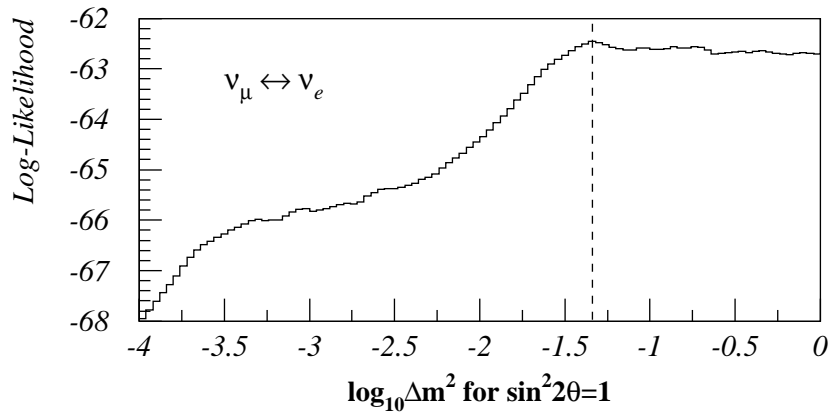
The quality of the fit in the $\nu_\mu \leftrightarrow \nu_e$ mode is good. The χ^2 probability (see Appendix B) is 35.4%. From the distribution of the maximum log-likelihood for 1000 experiments that were simulated at the data solution (see Appendix B), the probability for obtaining a value of likelihood below -62.5 is 38.1% (fig. 7.21) – the maximum log-likelihood for the $\nu_\mu \leftrightarrow \nu_e$ data fit is -62.46 .

Maximum of log-likelihood at	$\sin^2 2\theta = 1, \Delta m^2 = 0.046 \text{ eV}^2$
MC population at maximum: $A(\mu \leftrightarrow e)$	230.9 ± 27.2
MC population expected at maximum	$312.8 (\pm 20\%)$
ROCK population at maximum: $X(\mu \leftrightarrow e)$	53.9 ± 20.7
Value of log-likelihood at maximum	-62.46
Log-likelihood probability	38.1%
χ^2/ndf	$21.75 / 20$
χ^2 probability	35.4%

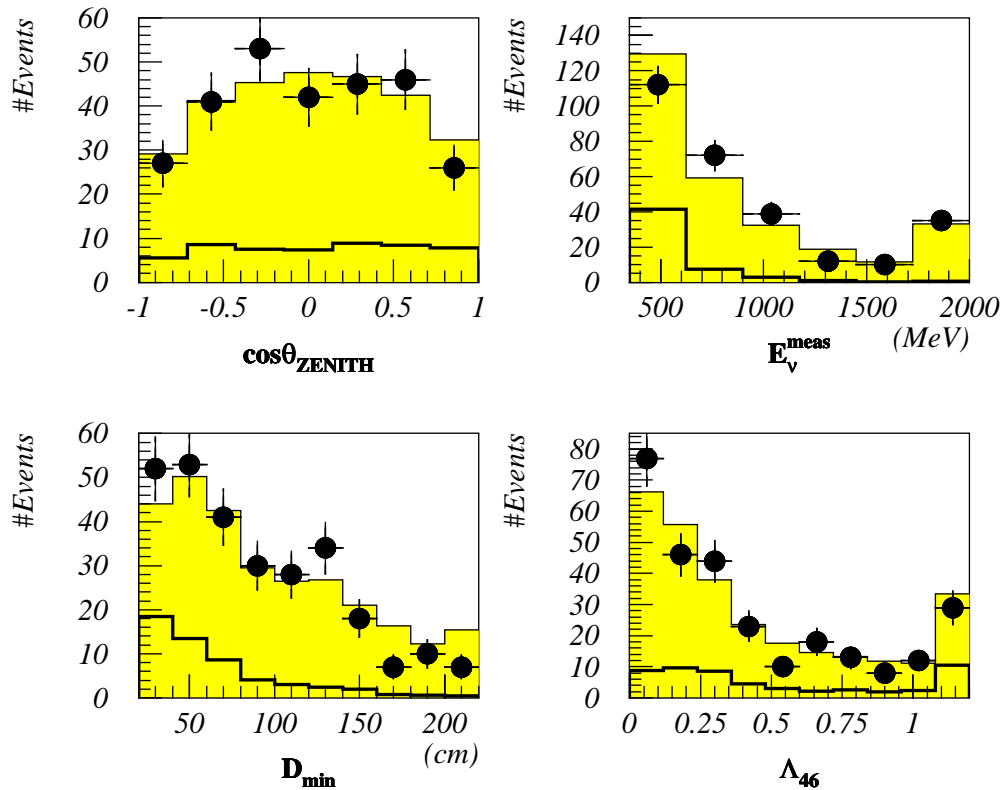
• **Table 7.7:** Results of $\nu_\mu \leftrightarrow \nu_e$ mixing multi-variable fit with background.



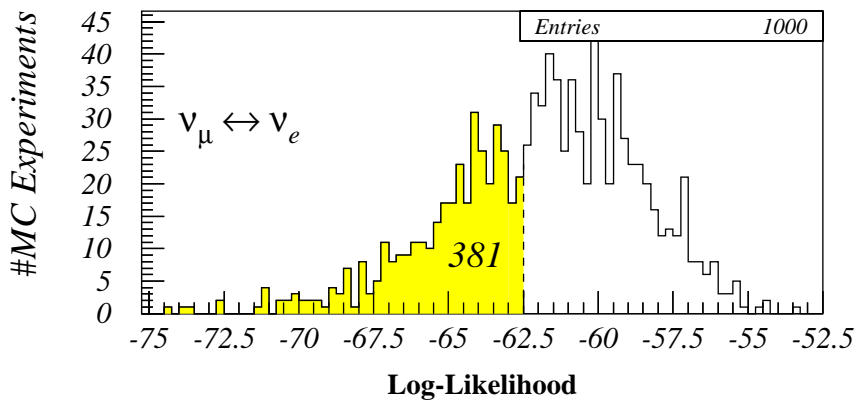
• **Figure 7.18:** Neutrino mixing parameters, Δm^2 and $\sin^2 2\theta$, limits for $\nu_\mu \leftrightarrow \nu_e$ oscillations mode, as determined by log-likelihood multi-variable fit. The 68%, 90%, 95% and 99% confidence level limits are shown.



• **Figure 7.19:** Variation of log-likelihood as a function of Δm^2 for $\sin^2 2\theta = 1$ and $\nu_\mu \leftrightarrow \nu_e$ mixing. The best fit (maximum) at $\Delta m^2 = 0.046 \text{eV}^2$ is indicated.



• **Figure 7.20:** Distributions of zenith angle, neutrino energy, depth and Λ_{46} flavour estimators for (i) the GOLD data (error bars), (ii) best fit MC ($\nu_{\mu} \leftrightarrow \nu_e$) plus ROCK model (shaded area) and (iii) ROCK, normalised to multi-variable fit solution (solid line).



• **Figure 7.21:** Distribution of log-likelihood at the maximum of the Δm^2 and $\sin^2 2\theta$ neutrino mixing parameter space. It has been obtained by fitting 1000 MC experiments whose truth is at the $\nu_{\mu} \leftrightarrow \nu_e$ solution of the data fit. Background has been added to each of these experiments – see Appendix B.

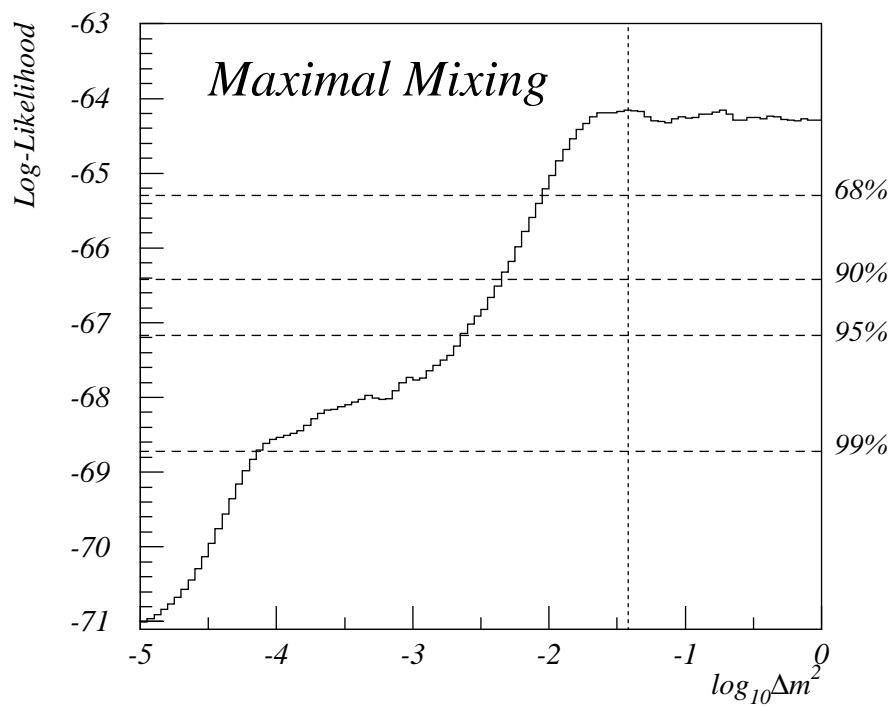
7.3.3 Three Generation Maximal Mixing

The data is fitted for neutrino mixing in the 3-generation maximal mixing mode [51]. The results are summarised in Table 7.8. The MC(maximal mixing) absolute normalisation from the experiment's exposure is in good agreement with the neutrino population calculated by the fit. The exclusion region as a function of Δm^2 for different confidence levels is shown in fig. 7.22. The data prefers $\Delta m^2 > 5 \times 10^{-3} \text{ eV}^2$ at a 90% confidence level, which includes the HPS solution at $\Delta m^2 = 7.2 \times 10^{-3} \text{ eV}^2$ [51][52]. As with the other two mixing modes examined in the previous sections, there is no bound in Δm^2 from above.

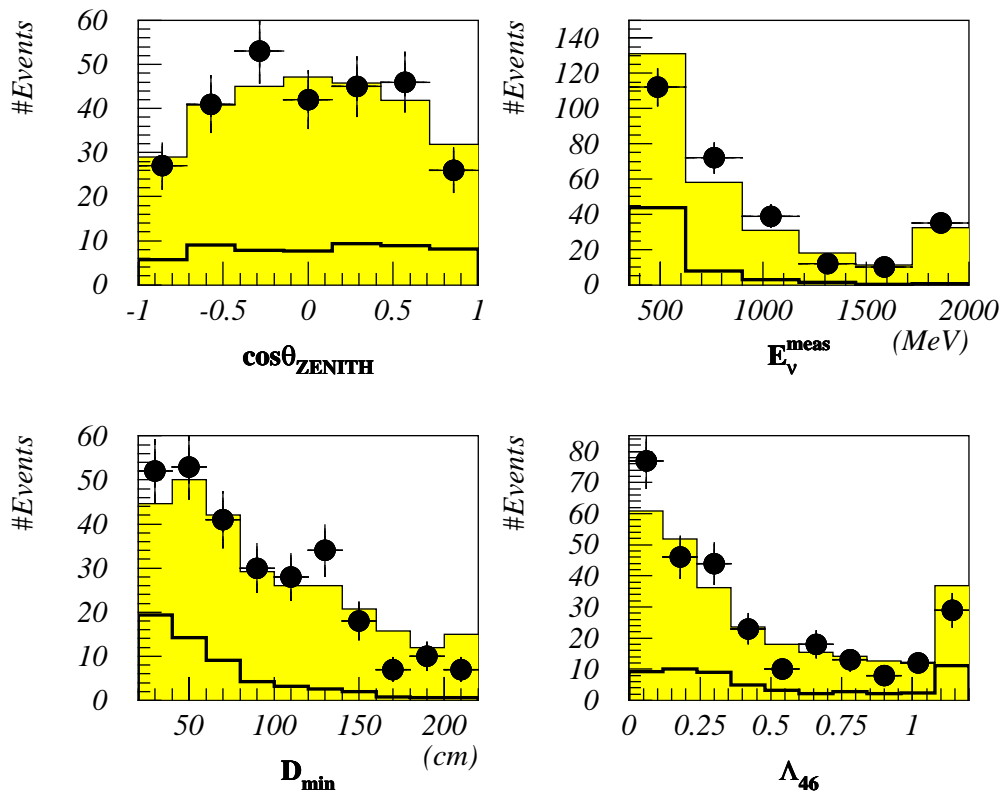
The maximal mixing model does not describe the data as well as the $\nu_\mu \leftrightarrow \nu_e$ and $\nu_\mu \leftrightarrow \nu_\tau$ hypotheses, at least in terms of the flavour estimator Λ_{46} (fig. 7.23): the GOLD data excess in the first bin is more prominent here than it is in the other two mixing modes. However, the effect is not as strong as to exclude the maximal mixing hypothesis. The fit is good: the χ^2 probability (see Appendix B) is 14.5% while the log-likelihood probability is 18.2% (fig. 7.24).

Maximum of log-likelihood at	$\Delta m^2 = 0.038 \text{ eV}^2$
MC population at maximum: $A(\text{max. mixing})$	224.9 ± 26.1
MC population expected at maximum	$240.4 (\pm 20\%)$
ROCK population at maximum: $X(\text{max. mixing})$	56.6 ± 20.7
Value of log-likelihood at maximum	-64.17
Log-likelihood probability	18.2%
χ^2/ndf	27.9 / 21
χ^2 probability	14.5%

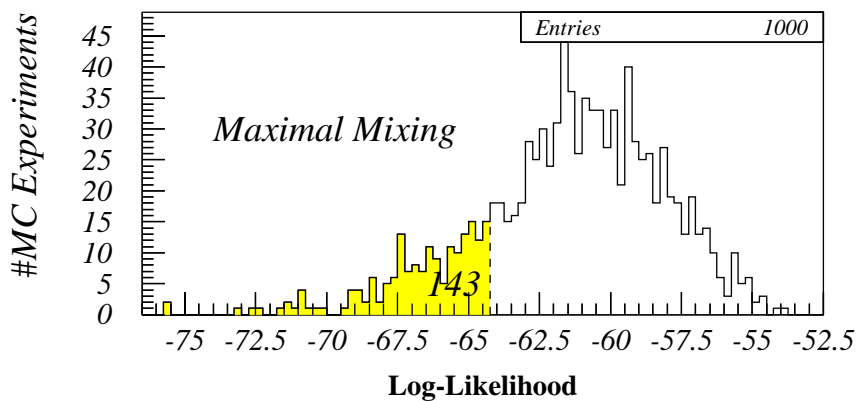
• **Table 7.8:** Results of maximal mixing multi-variable fit with background.



• **Figure 7.22:** Neutrino mixing parameter, Δm^2 , limits for maximal mixing mode, as determined by log-likelihood multi-variable fit. The 68%, 90%, 95% and 99% confidence limits are shown. Maximum is at $\Delta m^2 = 0.038\text{eV}^2$.



• **Figure 7.23:** Distributions of zenith angle, neutrino energy, depth and Λ_{46} flavour estimators for (i) GOLD data (error bars), (ii) best fit MC(maximal mixing) plus ROCK model (shaded area) and (iii) ROCK, normalised to multi-variable fit solution (solid line).



• **Figure 7.24:** Distribution of log-likelihood at the maximum of the Δm^2 neutrino mixing parameter space. It has been obtained by fitting 1000 MC experiments whose truth is at the maximal mixing solution of the data fit. Background has been added to each of these experiments – see Appendix B.

7.4 Conclusions

The automated analysis of 2.68 kTyears fiducial exposure (from August 26th, 1991 to December 22nd, 1996) of the data collected by the Soudan 2 experiment has been completed.

The following statements summarise the results:

- The atmospheric neutrino Ratio of Ratios has been calculated:

$$R = 0.62 \pm 0.14(\text{stat.}) \pm 0.05(\text{syst.})$$

- The anomaly is due to a low muon-like neutrino count rate rather than a high electron-like neutrino count rate.
- Alternatively, the data is compared to the Standard Model expectation in terms of a multi-variable fit. The probability that the Soudan 2 atmospheric neutrino data is compatible with Standard Model physics is low, namely 0.5%.
- The anomaly cannot be accounted for by background contamination, as it is demonstrated by the flavour composition of the background sample as a function of depth and shield multiplicity.
- The data has been compared with the $\nu_\mu \leftrightarrow \nu_\tau$, $\nu_\mu \leftrightarrow \nu_e$ and maximal mixing hypotheses, with log-likelihood probabilities of 30.4%, 38.1% and 18.2% respectively. For large mixing angle ($\sin^2 2\theta$ of unity) $\Delta m^2 > 5 \times 10^{-3} \text{ eV}^2$ at the 90% confidence level.
- There is no upper bound for Δm^2 because the data zenith angle distributions (for both flavours) are flat. Indeed, there is no compelling evidence in terms of the zenith angle for neutrino oscillations, which in turn pushes the accepted range of Δm^2 upwards.
- The collection of more data will reduce the statistical uncertainties and will help to clarify whether the small data deficit observed deep in the detector is a statistical fluctuation or a real effect.

- Finally, improvement in the performance of the neutrino direction estimator, for muon neutrino interactions in particular, will enhance the experimental neutrino L/E_ν phase resolution and will allow us to search for neutrino oscillations more efficiently.